CHAPTER 3

MULTIMODE PIC SIMULATION OF A GYROKLYSTRONAMPLIFIER

CHAPTER 3

MULTIMODE PIC SIMULATION OF A GYROKLYSTRONAMPLIFIER

3.1. Introduction

The beam-wave interaction mechanism in the gyro-devices are quite complex, and the operation of the device at higher harmonics leads to the mode competition from the nearby higher harmonic modes and fundamental harmonic modes. Therefore, in the previous chapter, the self-consistent multimode nonlinear analysis of the gyroklystron amplifier has been developed in order to understand its multimode beam-wave interaction mechanism. The single-mode nonlinear analysis describes the presence of single mode inside the RF interaction cavity, however in order to predict the effect of various competing modes on the output behavior of the device, such as, RF output power, and efficiency, nonlinear multimode analysis of the device have been carried out. Hence, multimode approach is more realistic and provides complete description of the mechanism of beam-wave interaction in the device. Based on the developed multimode nonlinear analysis, the numerical code has been written which is then used to benchmark the published experimental values. For numerical benchmarking, a Ka-band gyroklystron amplifier operating in the second harmonic TE_{02} mode for radar application has been typically selected [Antakov *et al.* (2011)].

However, numerical analysis gives the comprehensive representation of the device beam-wave interaction mechanism without incorporating the practical design constraints. Therefore, nowadays, considerable interests have been grown in the detailed and accurate time-dependent PIC simulation techniques that aid in in-depth understanding

and gives insight into the physics governing the operation of the fast-wave electron-beam devices including, gyrotrons, gyro-TWTs, gyroklystrons, etc. [Barroso *et al*. (1999), Kory and James (2009), Kumar *et al*. (2011), Reddy *et al*. (2008), Reddy *et al*. (2010), Wu *et al*. (1996)]. Nevertheless, the advent of high speed computers leads to the wide use of simulation and modeling techniques. These techniques offer more efficient vision of the device EM behavior by integrating the practical design constraints and provide the validation and optimization of the design parameters without fabricating the actual device. Numerical simulations also provide in-depth investigation of the nonlinear effects for different schemes and therefore facilitate the overall design of the electron-beam devices.

There are several codes, such as, MAGIC [Gopplen *et al.* (1995)], CHICPIC [Zhou *et al.* (2008)], and ARGUS [Petillo *et al.* (1994)] in which the real performance of the amplifier could be realized under practical condition, i. e., in the presence of electron beam (under hot condition). The simulation techniques are based on the FDTD-PIC step in which the finite difference time-domain (FDTD) scheme is used to calculate the fields and the particles are specified by the particle-in cell (PIC) scheme. As per the state of art, both 2D and 3D PIC simulation codes, like, CHIPIC, 2D MAGIC are used for gyroklystrons in past [Choi (1998), Zhou *et al.* (2008)]. A 28GHz, 200kW five-cavity gyroklystron amplifier was designed by Choi using 2D MAGIC code [Choi (1998)]. Wang *et al.* investigated the beam-wave interaction behavior in a four-cavity gyroklystron amplifier operating in TE_{021} mode using simulation technique "MAGIC" code [Wang *et al.* (2008)]. Later on, the four-cavity 30GHz gyroklystron amplifier is designed through optimization of various parameters using PIC simulation technique [Lei (2009)]. Xu *et al.* used the PIC simulation for validating their self-consistent analytical results obtained for W-band four-cavity gyroklystron amplifier [Xu *et al*. (2012)]. Another simulation code, MAGY is an

example of a hybrid code which is developed by University of Maryland and Naval Research Laboratory, Washington, DC for the simulation of slow and fast-wave devices [Botton *et al*. (1998)]. The code was initially designed for the modeling of gyrotron oscillators and then the code has been successfully applied in a series of gyro-amplifiers for radar applications in the United States for the device analysis and design [Nguyen *et al*. (2000)]. The implementation of the gyroklystron amplifiers using MAGIC software has been effectively studied and reported [Chauhan *et al*. (2013)]. But the limitation of MAGIC software is that it can be observe the signal growth corresponding to the single mode only. Since the present work is focused on the time-dependent multimode behavior of the device, another commercial 3D PIC simulation code, CST Microwave studio that allows both the fields and the particles to be modeled in the time domain [CST user's manual (2013)] and overcomes the limitation of the MAGIC software by providing the setting to monitor the signal growth and output power in all the possible modes present in the cavity. In the present work, the multimode behavior of an experimentally reported Ka-band second harmonic three-cavity, gyroklystron amplifier [Antakov *et al.* (2011)] is studied using a commercially available GUI based 3D simulation code "CST Particle Studio". The simulated results are also verified through the analytical results obtained in the previous chapter, i. e., Chapter 2.

This chapter of the thesis is organized as follows. In Section 3.2, the basic approaches to the CST particle studio tool for PIC simulation and its features are discussed. Section 3.3 deals with the modeling of the RF interaction structure of the gyroklystron amplifier in detail and the multimode beam-wave interaction behavior in a gyroklystron amplifier is investigated through the simulated results. Further, the validation of the simulated results with the earlier reported experimental values [Antakov *et al.* (2011)] and

the analytical results are discussed in Section 3.4. Also, the sensitivity of the RF output power, gain, and efficiency on the various system parameters are described. The relevant conclusions are drawn in Section 3.5.

3.2. PIC Simulation Code 'CST'

Today microwave engineers depend heavily on the flexible simulation tools to analyze the complete behavior of the design of the new device and to optimize the device design parameters. The computer methods to solve electromagnetic problems mainly fall into three categories: numerical, analytical, and expert methods. Analytical methods are applied to simple and uniform and geometries because it applies certain assumptions regarding the geometry, for simplifying the problem. However, numerical methods can be applied to complex and heterogeneous geometrical structures, hence requires lots of computations and is more powerful tool. In expert systems, the RF fields are not calculated directly, but instead it evaluates values for the desirable parameters. There are mainly two types of numerical methods for solving the electrical methods. The first category is Time-Domain (TD) method which includes Finite-Difference Time-Domain (FDTD) method, Finite-Element Time-Domain (FETD) method, and Finite-Volume Time-Domain (FVTD) method. The second type is Frequency-Domain method which includes Method of Moments (MoM), and Finite Integration Technique (FIT). Out of the above discussed methods, the FIT method has been extensively used for electromagnetic applications over an extremely wide range of frequencies, from DC to THz. The "CST Microwave Studio" is a general purpose electromagnetic simulator based on the finite integration technique (FIT) and which was first proposed by Weiland in 1977. "CST Particle Studio" is a specialized module for the fast and accurate analysis of charged particle dynamics in 3D

electromagnetic fields and is an efficient tool for performing simulation of interaction between electromagnetic fields and charged particles.

3.2.1. PIC Simulation Description

CST Particle Studio uses finite integration numerical method as solving technique and uses hexahedral/tetrahedral meshing for discretizing the computational domain. Post-processing module for the diagnosis of results is its salient feature. It provides users to employ six different field solvers, electrostatic, magnetostatic, eigenmode solver, particle tracking solver, particle in cell solver (PIC), and Wakefield solver. The eigenmode solver is dedicated to the simulation of closed resonant structures. In cases of loss-free strongly resonant structures, in which the fields (the modes) are to be calculated, the eigenmode solver is very efficient. The eigenmode solver cannot be used with open boundaries or discrete ports [CST user's manual (2013)]. Magnetostatic solver can be used for static magnetic problems while electrostatic solver can be used for static electric problems. Both of these solvers utilizes feature of open boundary conditions as well as the electric and magnetic open boundary condition. These help to reduce the number of mesh nodes, when problems in free space are simulated. The stationary particle tracking solver tracks particles based on the Lorentz Force equation in pre-calculated electromagnetic fields. These fields can be either electrostatic, magnetostatic or eigenmode fields. A self-consistent electrostatic field is calculated using gun-iteration implemented which considers the reaction of the particle movement to the electrostatic potential distribution. Particle sources can be defined at arbitrary surface of solids that emits particles according to the predefined emission models. The major task for the tracking solver is to calculate the particle trajectories, the self-consistent electrostatic field, the space charge distribution, and

the particles' current. These results appear automatically in the navigation tree after the solver run. The particle tracking solver also offers the tracking of different types of particle from different sources independently. Thus, multibeam guns or the parallel simulation of particle beams can be simulated. The computation of wake potentials of charged particle bunches can be performed using the Wakefield solver. The Wakefield solver provides features such as wake-potential, beam frequency, impedance, and loss factors. For the designing of particle-accelerators, wake potentials provide important information. The PIC solver simulates the evolution of charged particles in self-consistent electromagnetic fields. Moreover, in the PIC simulation, the static or analytic field distributions can easily be added. Feature of PIC solver includes the charged particles emission from arbitrary surfaces or single points.

Similar to other PIC codes, CST Particle Studio involves four major steps before proceeding for the solution of beam-wave interaction problems. The basic steps in observing RF interaction structure in the beam present case using PIC solver are discussed below. In the CST particle studio, 2D cross-sectional view of the RF interaction structure needs to be defined for which simulation has to be performed. For the beam absent case, cavity is simulated using the eigenmode solver of the CST microwave studio. After defining the geometry, simulation frequency range of simulation should be defined as per the operating region of the cavity. In the ‘quick start guide’ feature of the software code, the corresponding relevant solver module, the important steps of performing the simulation can be determined. A waveguide port is defined at the output section of the cavity to determine the signal amplitude corresponding to the different modes. A desired cross section of an electron beam with the desired beam parameters is injected into the electromagnetic structure, in order to make the interaction between the beam and the RF

signal. The beam parameter i. e. beam radius is evaluated according to the circuit dimension, i. e., cavity radius and the desired operating mode. The parameters for developing the electron beam are also defined.

The external magnetic field must be assigned to focus the electron beam in a well defined trajectory inside the interaction structure. To understand the behavior of an electromagnetic device, it is necessary to have insight of the electromagnetic field distribution. Thus, required frequency points are defined at which solver will record the fields and these field samplers are called Field Monitors. These are mainly of two types: electric field (*E*-Field) monitor and magnetic field (*H*-Field) monitor in which the electric field distribution is investigated through *E*-Field monitor and magnetic field distribution is investigated through *H*-Field monitor. The monitor of electric and magnetic field as well as power inside the cavity are defined in the specified dialog box. Particles are also monitored in 2D or 3D planes to have the information about the perturbation of the particles in terms of energy or phase, and bunching phenomena. For this, the phase space monitors are defined. Using the 2D particle monitor, the particles are monitored for their momentum, position etc. at a set of interval of time, i. e., over the full time or partial time of simulation to acquire the modulation of energy or momentum among particles.

3.3. PIC Simulation of a Three-Cavity Gyroklystron Amplifier

In order to validate the developed analytical approach described in Chapter 2, the commercial 3D PIC code "CST Particle Studio" is reconfigured for the gyroklystron physical structure and electrical parameters to study its multimode beam-wave interaction behavior. The PIC simulation of a gyroklystron amplifier mainly consists of three steps. Firstly, RF interaction structure of a gyroklystron amplifier is modeled for simulation using

the relevant design parameters. Secondly, the desired mode of operation at desired frequency is selected by simulating the structure in the absence of beam (cold analysis) using Eigenmode solver. Lastly, the performance of the device in terms of RF output power and gain are obtained by simulating the structure in the presence of beam (hot analysis). The signal amplitudes corresponding to all the possible modes in the cavity are obtained to investigate the multimode interaction behavior of the device.

Table. 3.1: Design parameters of 32.3GHz, second harmonic, three-cavity gyroklystron amplifier [Antakov *et al*. (2011)].

Parameters	Specifications
Operating Mode	TE_{02}
Beam Voltage (V_b)	70kV
Beam Current (I_b)	20A
Velocity Pitch Factor (α)	1.1
Beam radius (R_b)	$0.43R_w$
DC Magnetic Field (B_0)	0.656T
Input Cavity Length	16mm
Buncher Cavity Length	15mm
Output Cavity Length	22.3mm
Quality factor of input cavity (Q_1)	600
Quality factor of buncher cavity (Q_2)	450
Quality factor of output cavity (Q_3)	1050

The design parameters considered for the present simulation are taken from the reported experimental results of [Antakov *et al*. (2011)] as shown in Table 3.1. In the hot beam simulation, a gyrating electron beam with 70keV energy and velocity ratio (α) = 1.1 is imported at the input end of the cavity. With a 4.4mm beam radius, electron beam gets coupled to the first radial maximum of the operating TE_{021} mode in the resonator. The

desired frequency of operation can be confirmed by taking the Fourier transform of time varying field in hot beam analysis.

3.3.1. RF Interaction Structure Modeling

A 2D cross-sectional view of the RF interaction circuit of a three-cavity Ka-band second harmonic gyroklystron amplifier modeled in CST for PIC simulation is shown in Fig. 3.1 to study its beam-wave interaction mechanism. The material property of the cavity walls of the RF interaction structure is taken as copper with the conductivity of 5.8×10^7 S/m to reduce the ohmic losses in the structure and the background material is kept as vacuum during simulation. Several steps are then involved in the modeling of RF structure like, the radius of the cavity, radius of the drift section, resonating frequency, and the *Q*-factor.

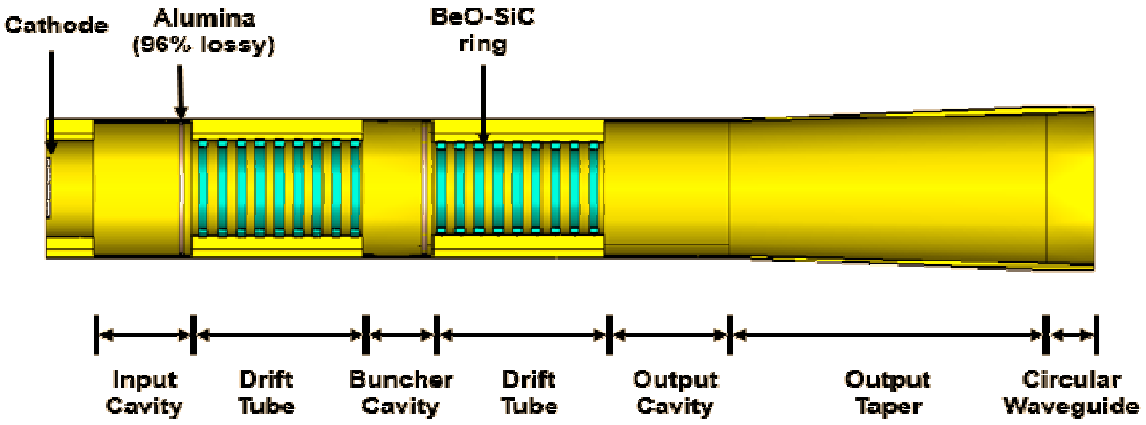

Figure. 3.1: Cross sectional view of the simulation model of the interaction circuit of gyroklystron amplifier.

The input cavity and buncher cavity is loaded with a lossy material (lossy alumina (96% lossy)) to achieve the desired quality factor. The *Q*-factor calculation is done by setting the *H*-field monitor. The drift tubes are loaded with lossy ceramic rings of BeO-SiC material to provide the complete isolation between the adjacent cavities. The field leaked from the cavities to drift region are absorbed and hence spurious oscillations get suppressed. Beryllium Oxide-silicon Carbide (BeO-SiC) with a relative permeability of $\varepsilon_r = 7.11 - j1.1$

and a relative permeability μ_r = 1 has been chosen as the dielectric material for the loaded section of the model because of its good thermal conductivity and due to its preference for high average power operation [Samartsev *et al.* (2011)]. The ceramic ring has length of 2mm and 1mm radial thickness. The phenomenon of energy transfer can be understood by analyzing the electron bunch formation. To visualize this, the phase space for energy of electrons is recorded by setting the phase space monitors. The cavity operation in the desired mode and frequency has been observed by setting the *E*-field monitor. The port is assigned at the end of the output taper to observe the signal corresponding to any mode.

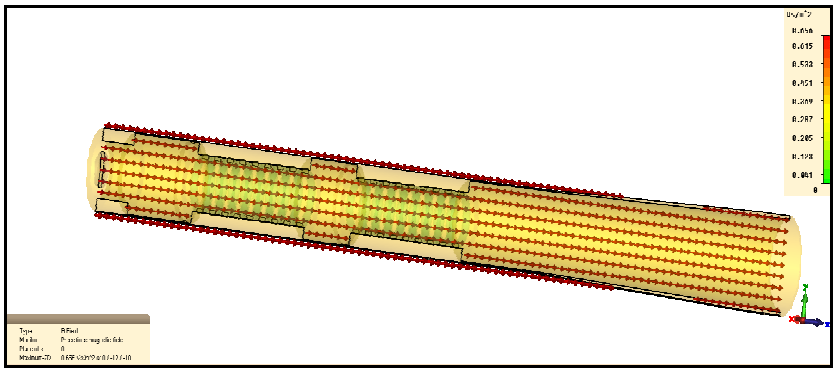

Figure. 3.2: Application of DC Magnetic field along the interaction structure.

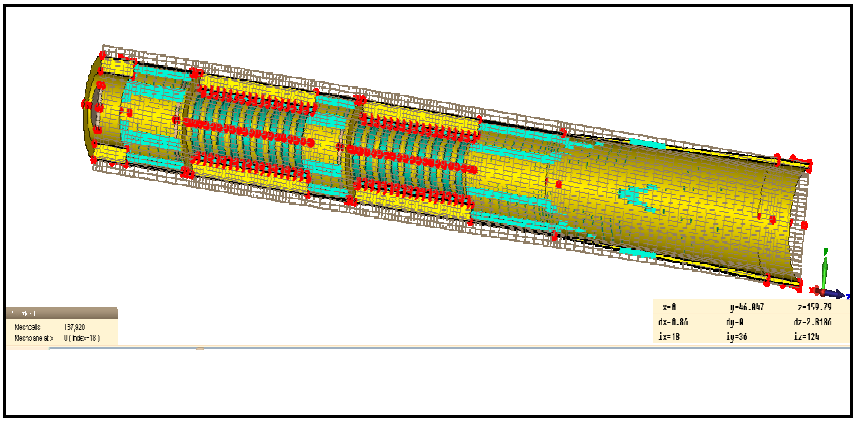

Figure. 3.3: Mesh distribution along the interaction structure.

The constant DC magnetic field of 0.656T is applied along the interaction structure as shown in Fig. 3.2. Proper meshing has to be considered for the discretization of the structure to obtain accurate results. To reduce the time of simulation and to improve the

efficiency of the device, tetrahedral meshing technique is used which increases the speed of computations with good accuracy and which is also very efficient even for the complex imported geometries. The size of mesh cells can be controlled by the lines per wavelength. In order to improve the accuracy in PIC simulation, the mesh size should be chosen wisely. Lines per wavelength and lower mesh limit should be kept so as to get good accuracy in lesser simulation time. In the present simulation, the automatic mesh generation technique is used in which the lines per wavelength is taken as 10 and lower mess limit as 10. This technique provides a minimum and maximum mesh step size of 0.2 mm and 1.00584 mm, respectively, which corresponds to the total number of mess cell of 4,87,750.

3.3.2. RF Cavity Simulation (Beam Absent Condition) — Eigenmode Study

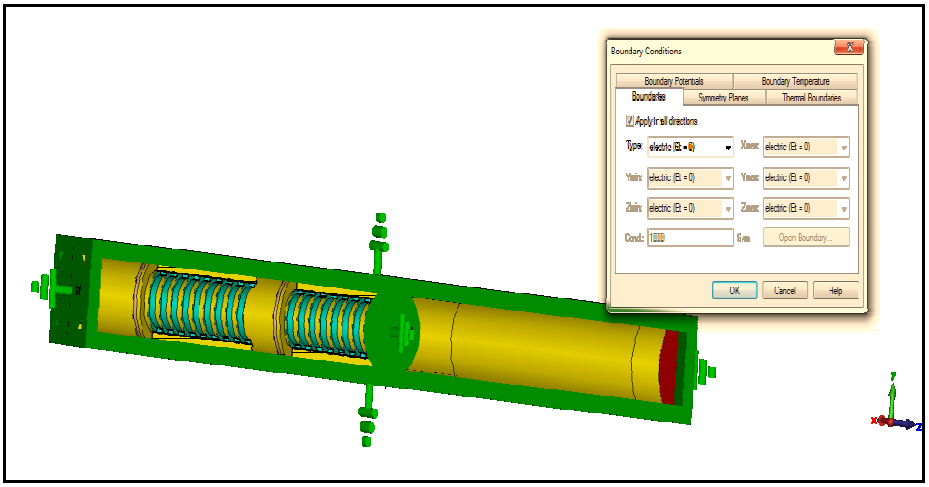

Figure. 3.4: Implementation of boundary conditions along the interaction structure.

Eigenmode analysis of the gyroklystron cavities is carried out before the PIC simulation using eigenmode solver to calculate eigenvalues (resonating frequencies) and eigenmodes (field patterns) in the absence of electron beam. In this technique, the electric field pattern is observed to confirm the presence of a particular mode inside the cavities. The tangential electric field component is considered as null ($E_t = 0$) as boundary condition while carrying out the eigenmode study as shown in Fig. 3.4.

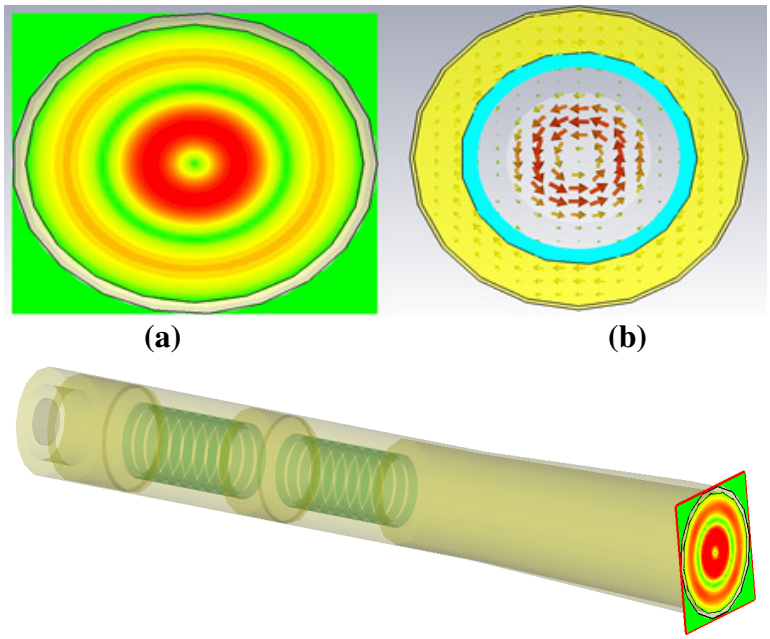

Figure. 3.5: Pattern of RF Electric field inside the gyroklystron input cavity **(a)** Contour plot, **(b)** Vector plot, and **(c)** Contour plot at the output port.

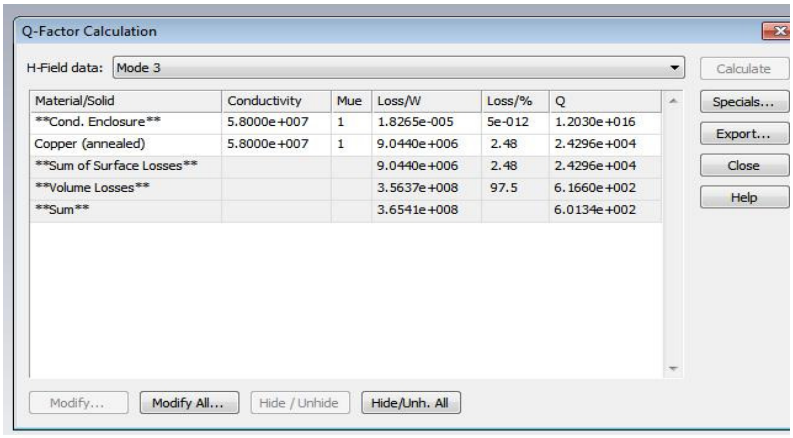

Figure. 3.6: *Q*-factor calculation in the input cavity.

Figure 3.5(a) shows the contour plot of pattern of RF electric field inside the gyroklystron input cavity, and Fig. 3.5(b) shows the vector plot of electric field inside the input cavity. From the Figure, it is observed that there are two variations in the radial direction and no variation in azimuthal direction which shows that the device is operating in the TE_{02} mode. The total loss calculation in a cavity is accessible through 2D/3D field processing → Loss

and Q calculation which includes the dielectric loss and the surface loss. As a consequence of this loss calculation, the Q factor of a cavity is achieved. Figure 3.6 shows the Q-factor calculation in the input cavity which is obtained by loading the cavity with lossy aluminium silicate (Alumina (96% lossy)) ring. The Q-factor in the input cavity is obtained as around 600. By following the similar procedure, the Q-factor in other cavities is calculated.

3.3.3. PIC Simulation of the RF Interaction Structure (Beam Present Condition) — Beam-Wave Interaction Study

After performing the beam-absent simulation, simulation is extended for beam-present case. Further, for the PIC simulation, electrons are considered as uniformly distributed azimuthally in the form of gyrating beamlets. In the time domain, the evolution of electrons in the presence of electromagnetic signal is observed along the axial direction of the RF interaction structure. The space charge effect on the electron beam is neglected, in order to facilitate the simulation process. An annular gyrating electron beam with the beam voltage of 70kV, and beam current of 20A with pitch factor of 1.1 is introduced at the left end of the interaction structure. The guiding centre radius is taken as 4.4mm. The gyrating electron beam then interacts self-consistently with the RF field present in the interaction structure. The electromagnetic field then changes the relativistic mass factor (γ) of electrons, depending on the electron phase relative to the wave, and hence results in phase slippage and bunching, with the corresponding current driving the wave. Initially, all the particles are assigned a constant energy value of 70keV and the current rise time is taken as 1 ns. To realize the more reasonable scenario, a kinetic spread can be directly introduced into the beam. For simulation, 8 beamlets and 0% axial velocity spread are considered. Electrons start to bunch as they drift along the RF interaction circuit and interact with the RF field. As a result, they transfer their energy in synchronism with the

Larmor gyration of the electrons. This results into the possible amplification of an electromagnetic wave at the cyclotron frequency.

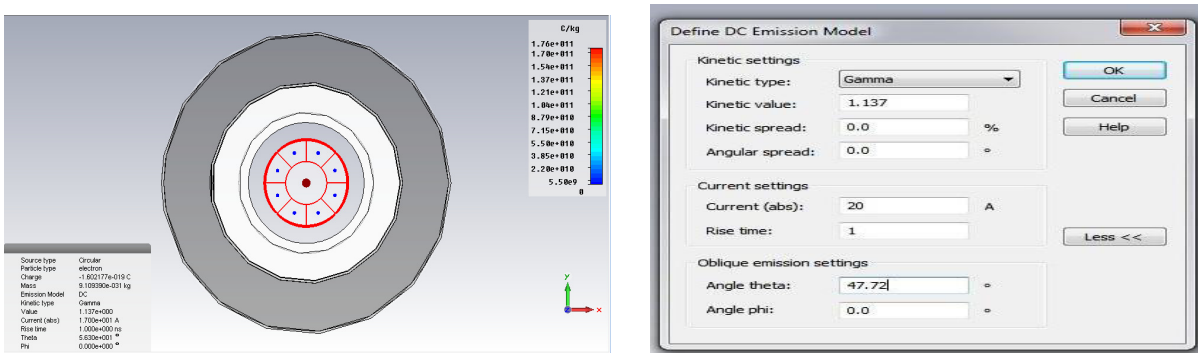

Figure. 3.7: Particle emission model.

3.3.3a Electron beam bunching

For the simulation of beam-wave interaction in the gyroklystron amplifier, eight beamlets are considered in the structure. However, these numbers of beamlets can be taken as larger but, of course, at the cost of time and memory consuming.

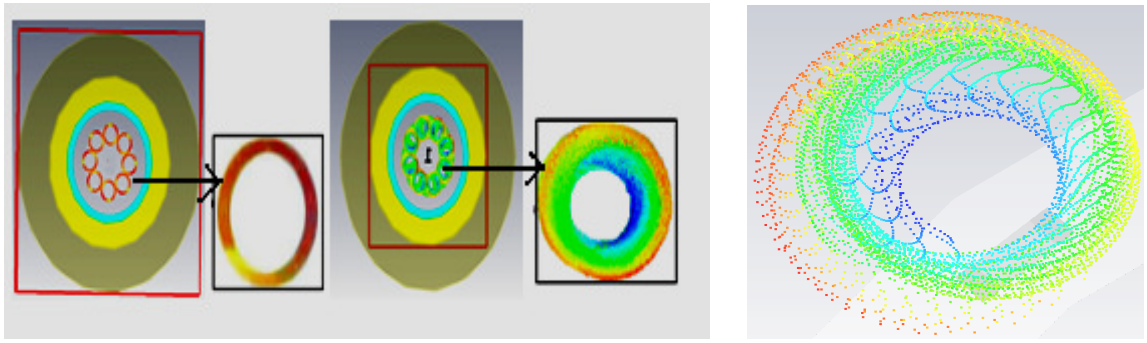

(a) (b)

Figure. 3.8: (a) Front view of electron beam with 8 beamlets before and after interaction, (b) Zoomed beamlet after interaction.

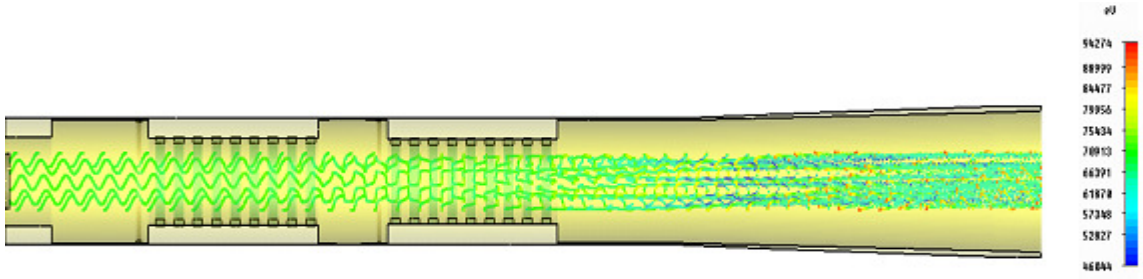

Figure. 3.9: Trajectory of electron beam from input port to output port during interaction.

The cross-section of the electron beam with 8 beamlets before and after RF interaction are shown in Fig. 3.8(a). Figure shows that before interaction, all the 8 beamlets are uniformly distributed with the fixed guiding center radius and their energies are equal at the starting of the interaction process. During the beam-wave interaction process, the electrons are not uniformly distributed and the bunching of electron particles lead to the change in their Larmor radius which is clearly shown in the zoomed beamlet in Fig. 3.8(b). Figure 3.9 shows the trajectory of the electron particles from the input port to the output port along the interaction length. It is clear from the figure that, during the beam-wave interaction process, the presence of RF field perturbs the momentum of electron-beam resulting in the bunch-formation at the output cavity.

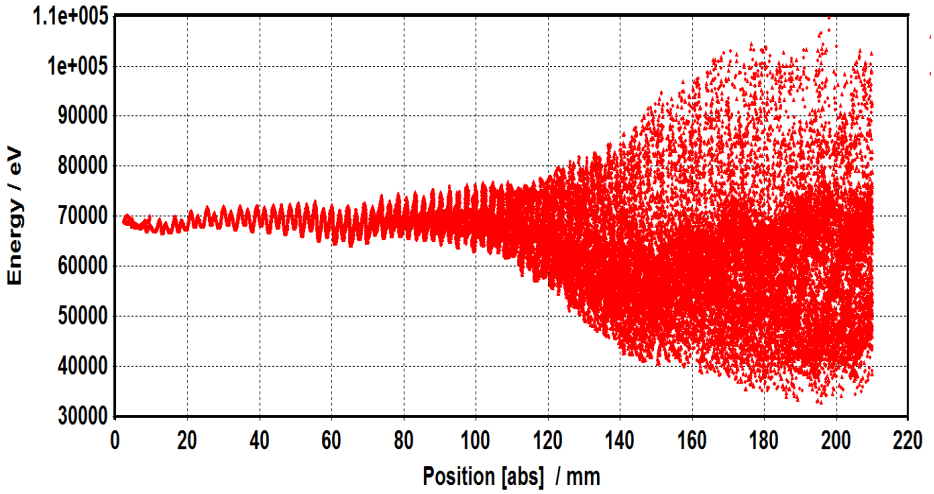

Figure. 3.10: Evolution of particles energy along the device axis.

The evolution of the electron energy along the interaction region is shown in Fig. 3.10. It can be seen that initially all the electrons have the same energy of 70keV but with time, the net energy of particles get perturbed along the cavity length due to the interaction with the RF field. At the output end of the cavity, majority of particles have lower energy which indicates that the net energy is transferred from the electrons to the RF wave, hence results in the amplification of the RF wave.

3.3.3b RF field pattern

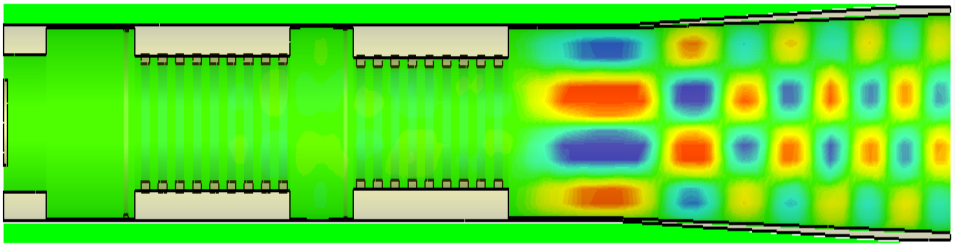

Figure. 3.11: Contour plot of the electric field pattern of TE_{02} mode along the axial length of the interaction circuit.

The contour plot of the electric field pattern along the axial length of the interaction circuit is shown in Fig. 3.11. It is observed that no propagation of the RF field is observed in the input cavity, while the intensity is slightly more in the buncher cavity. It can be seen that, in the output cavity, the RF field strongly resonates forming a standing wave while in the output taper, the RF field is present forming a traveling wave. From the contour plot of the electric field pattern, it clearly indicates that the TE_{02} mode is propagating along the axial length of the interaction circuit.

3.3.3c Output RF signal and power

The temporal growth of the field amplitude for the operating TE_{02} mode and the other nearby competing modes has been shown in Fig. 3.12.

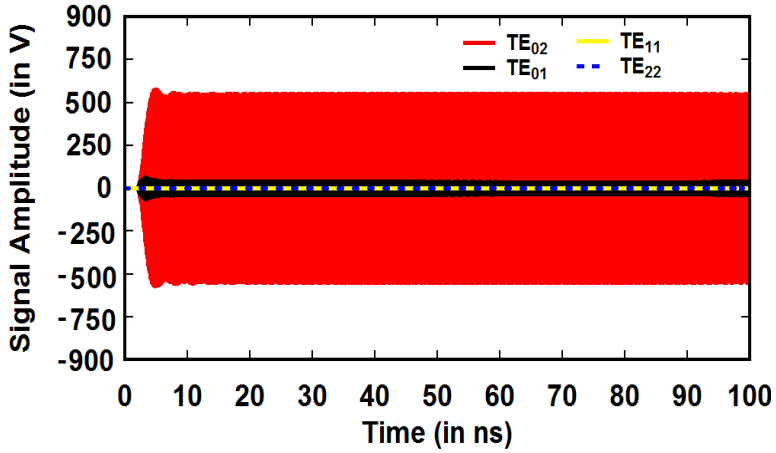

Figure. 3.12: Temporal growth of the EM signal in the operating TE_{02} mode and the nearby competing modes.

The output time signal corresponding to TE_{02} mode has the highest amplitude than all other modes at the applied DC magnetic field B_0 = 0.6555T and the mode competition is mainly observed due to the fundamental harmonic TE_{01} mode. The EM power growth approaches the saturation level at a time beyond 10ns.

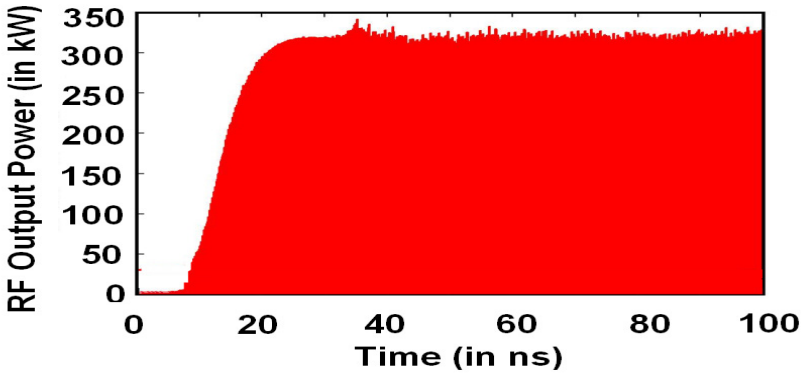

Figure. 3.13: Temporal output power growth in the TE_{02} mode at the output cavity.

After the template based post processing in CST particle studio, the saturated RF output power has been obtained as ~315kW with an electronic efficiency of 22.5% for a 70kV, 20A electron beam with a velocity ratio of 1.1. The gain of the device is obtained as ~26dB (Fig. 3.13).

3.4. Parametric Analysis and Validation

Using the PIC simulation, the parametric analysis of the gyroklystron amplifier is carried out for the device performance evaluation in terms of gain, bandwidth, and efficiency. Figure 3.14 shows the RF output power and gain as a function of RF input power for beam voltage corresponding to 65kV and beam current corresponding to 16.2A at 32.32GHz center frequency. It is clear from the figure that the RF output power increases rapidly with the increasing input power when the input power is less than about 2.0kW and then reaches saturated value around 225kW corresponding to 20.5dB gain. The results obtained from PIC simulation are validated with the reported experimental results

[Antakov *et al.* (2012)] and are found to be in agreement within 2% and the time-dependent multimode analysis within 3%. The 3dB bandwidth of the device is obtained by plotting

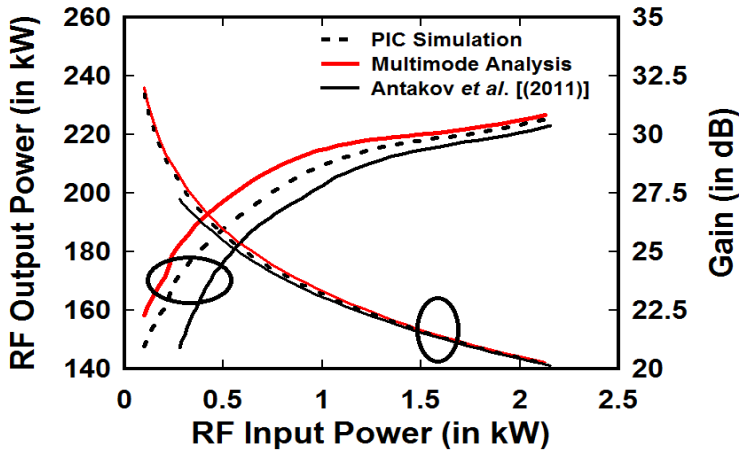

Figure. 3.14: RF output power and gain variation with driver power (for 65kV beam voltage, 16.2A beam current and 32.32GHz center frequency).

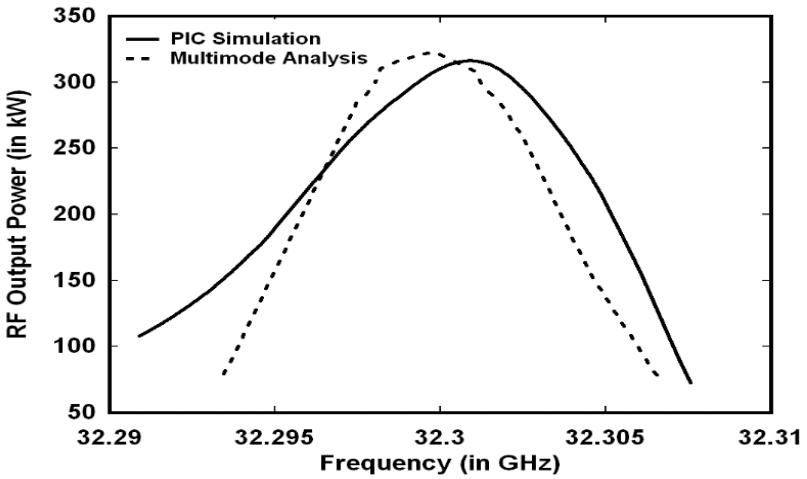

Figure. 3.15: Variation of RF output power and efficiency with driver frequency.

the variation of RF output power with frequency (Figure 3.15). It is clear from the figure that the gyroklystron amplifier achieved around 315kW RF output power and around 22.5% electronic efficiency at 32.3GHz center frequency with ~0.038% (11MHz) bandwidth. The PIC results obtained are found to be in close agreement with the analytical results obtained within 3%.

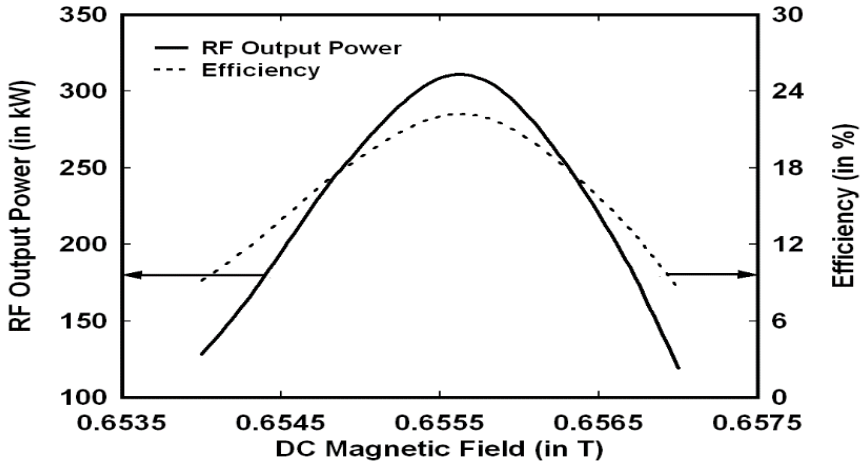

Figure. 3.16: Variation of RF output power and efficiency with DC magnetic field.

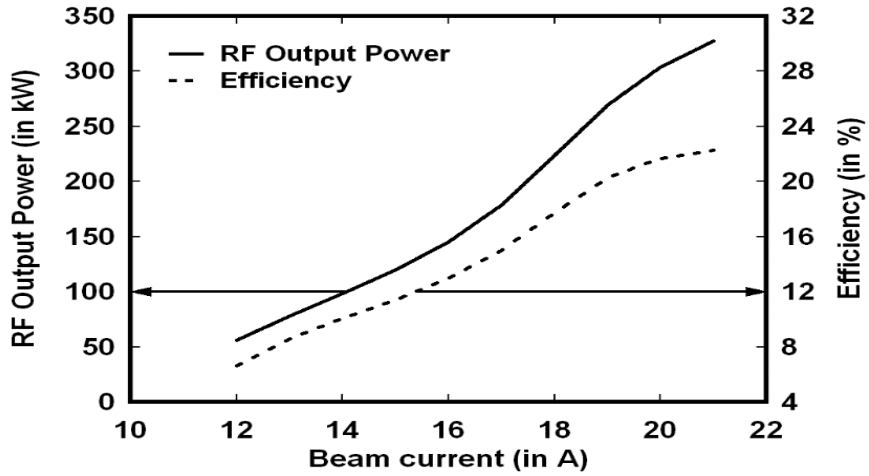

Figure. 3.17: Variation of RF output power and efficiency with beam current.

Figure 3.16 shows the variation of RF output power and electronic efficiency with DC magnetic field. The energy modulation and the phase bunching phenomenon are directly affected by the difference between the cyclotron frequency and the frequency of the electromagnetic wave. Since, the cyclotron frequency is decided by the applied DC magnetic field; hence the variation of the static magnetic field has a strong affect on the performance of the device. It is clear from the figure that the 315kW peak output power is obtained at the DC magnetic field around 0.6555T and the RF output power is 128kW and 119kW, respectively, when the magnetic field strength is 0.654T and 0.657T, and hence

sensitive to the variation in DC magnetic field in case of second harmonic gyroklystron amplifiers.

The variation of RF output power and electronic efficiency with beam current is shown in Fig. 3.17. It is clear from the figure that the peak output power of 315kW with 22.5% electronic efficiency is obtained at the beam current of 20A. Efficiency decrement at higher value of beam current is mainly due to the operation of the device very near to the start oscillation current.

3.5. Conclusion

To further validate the developed multimode analysis, the PIC simulation of the same experimental three-cavity Ka-band second harmonic gyroklystron amplifier as considered in Chapter 2 has been made in this chapter. The 3D PIC simulation procedure of the gyroklystron amplifier, reconfiguring the commercially available "CST Studio Suite" has been carried out. The RF interaction structure has been modeled for the experimental device parameters. In the PIC simulation, cold (beam absent) and hot (beam present) electromagnetic behavior of an all metal interaction structure have been demonstrated. Cold simulation has been performed using eigenmode solver to examine the cavity specific mode and frequency of operation. Using cold simulation, a well-defined TE_{02} mode has been observed in the cavity at 32.3GHz resonant frequency. Field distributions obtained in terms of vector and contour plots along the cavity dimensions confirm the operating TE_{02} mode of operation. Further, beam-present (hot) simulation has been performed to study the beam-wave interaction behavior in terms of RF output power and electronic efficiency. The electron beam trajectory along the interaction length has been observed which indicates that the presence of RF field perturbs the momentum of electron-beam resulting in the

bunch-formation. Particles energy and phase plots have been observed during the beam-wave interaction process of the gyroklystron amplifiers. These plots clearly demonstrate bunching of the particles in their Larmor radius of each beamlets and the energy transfer phenomena to the RF field. In the present PIC code, the temporal growth of the field amplitude for the operating TE_{02} mode and the other nearby competing modes present inside the RF interaction circuit can be observed. Hence, this simulation tool also provides a reasonable picture similar to the multimode analysis. It has been demonstrated that the interaction circuit takes some time to settle in the TE_{02} mode due to the competition from the nearby modes. From the PIC simulation, the RF output power has been obtained as ~315kW at 32.3GHz. The gain of the device has been calculated as ~26dB with an efficiency of ~22.5. Finally, simulation results are benchmarked with the previously reported experimental results and the analytical results obtained in Chapter 2 which are found to be in close agreement within 5%.